Supplement of Atmos. Meas. Tech., 16, 2431–2454, 2023
https://doi.org/10.5194/amt-16-2431-2023-supplement

Atmospheric Measurement Techniques
Open Access
EGU

Supplement of

Satellite remote-sensing capability to assess tropospheric-column ratios of formaldehyde and nitrogen dioxide: case study during the Long Island Sound Tropospheric Ozone Study 2018 (LISTOS 2018) field campaign

Matthew S. Johnson et al.

Correspondence to: Matthew S. Johnson (matthew.s.johnson@nasa.gov)

Table S1. Auxiliary information used for air mass factor (AMF) calculations for NO_2 and HCHO retrievals from NASA OMI, QA4ECV OMI, and TROPOMI.

	NO_2		
Algorithm component	**NASA OMI**	**QA4ECV OMI**	**TROPOMI**
Surface Albedo	Daily geometry-dependent surface Lambertian equivalent reflectivity (GLER) data	Climatological Lambertian equivalent reflectivity (LER) from OMI v3 surface reflectance	Climatological LER from OMI v3 surface reflectance
Cloud Pressure/Fraction	Updated OMI Cloud Data Product O2–O2 cloud product (OMCDO2N) from the GLER product	OMI O2–O2 product (OMCLDO2)	O_2-A band from FRESCO+ wide approach
Cloud Radiance	VLIDORT-based lookup table	bePRO/LIDORT-based lookup table	Doubling-Adding KNMI (DAK) lookup table
Scattering Weights	VLIDORT	bePRO/LIDORT	DAK
A Priori Profiles	Monthly GMI profiles at 1°×1.25°	Daily profiles from TM5-MP at 1°×1°	Daily profiles from TM5-MP at 1°×1°
	HCHO		
Algorithm component	**NASA OMI**	**QA4ECV OMI**	**TROPOMI**
Surface Albedo	Climatological LER from OMI v3 surface reflectance	Climatological LER from OMI v3 surface reflectance	Climatological LER from OMI v3 surface reflectance
Cloud Pressure/Fraction	OMI O2–O2 product (OMCLDO2)	OMI O2–O2 product (OMCLDO2)	Operational cloud product from a Lambertian cloud model (CRB)
Cloud Radiance	VLIDORT-based lookup table	VLIDORT-based lookup table	LIDORT-based lookup table
Scattering Weights	VLIDORT	VLIDORT	LIDORT
A Priori Profiles	Monthly climatology from GEOS-Chem at 2°×2.5°	Daily profiles from TM5-MP at 1°×1°	Daily profiles from TM5-MP at 1°×1°

Table S2. Physical parameterizations used in WRF model simulations.

Physical process	Parameterization (Reference)
Long-wave radiation	Rapid Radiative Transfer Model for General Circulation Models (RRTMG) (Iacono et al., 2008)
Short-wave radiation	RRTMG (Iacono et al., 2008)
Microphysics	Morrison double-moment (Morrison et al., 2010)
Cumulus parameterization	Kain–Fritsch version 2 (Kain, 2004)
Land surface model	Pleim–Xiu LSM (Pleim and Xiu, 1995)
Surface Layer	Pleim–Xiu surface layer (Pleim, 2006)
Planetary boundary Layer	ACM2 (Pleim, 2007)

Table S3. Statistical evaluation of NASA OMI, QA4ECV OMI, and TROPOMI retrievals of tropospheric column HCHO. Statistics presented are median bias ± bias standard deviation and NMB (%).

NASA OMI (0.15° × 0.15°)				QA4ECV OMI (0.15° × 0.15°)			
	Clean	Polluted	Highly Polluted		Clean	Polluted	Highly Polluted
Bias*	2.8±6.2	4.6±7.9	-2.3±9.2	Bias*	2.7±7.3	2.1±8.7	-3.8±7.4
NMB	75.1	30.3	-8.9	NMB	72.1	13.7	-14.6
TROPOMI (0.15° × 0.15°)				TROPOMI (0.05° × 0.05°)			
	Clean	Polluted	Highly Polluted		Clean	Polluted	Highly Polluted
Bias*	3.1±1.4	1.8±4.4	-2.2±4.8	Bias*	2.4±2.3	1.3±6.5	-2.7±7.0
NMB	78.1	12.5	-8.7	NMB	60.9	8.5	-10.1

*bias units are $\times 10^{15}$ molecules cm^{-2}.

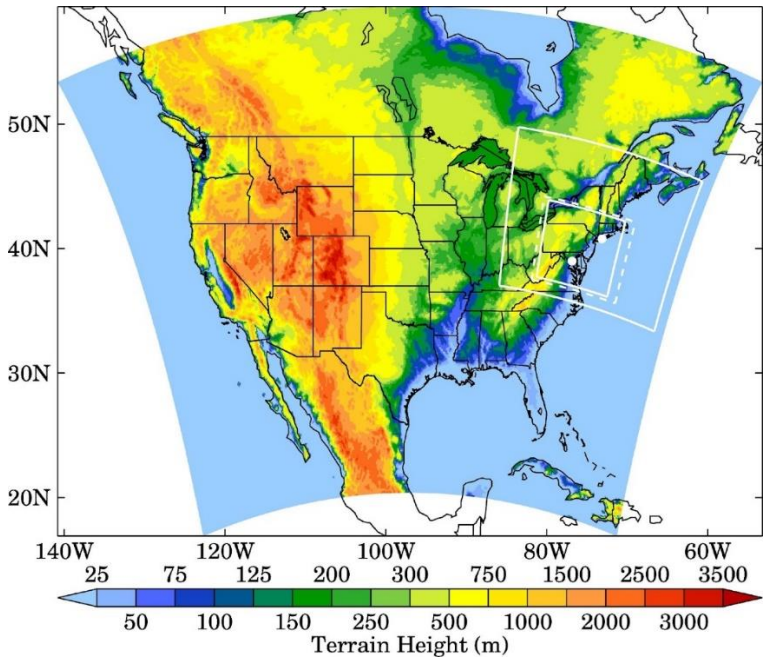

Figure S1: WRF-CMAQ modeling domains applied in this study. The white solid lines show the boundaries of the two CMAQ domains while the dotted white lines represent the boundary of the inner WRF domain. Terrain height for the outer WRF domain is also shown. The two white dots mark the regions of focus in the OWLETS-2 and LISTOS 2018 campaigns.

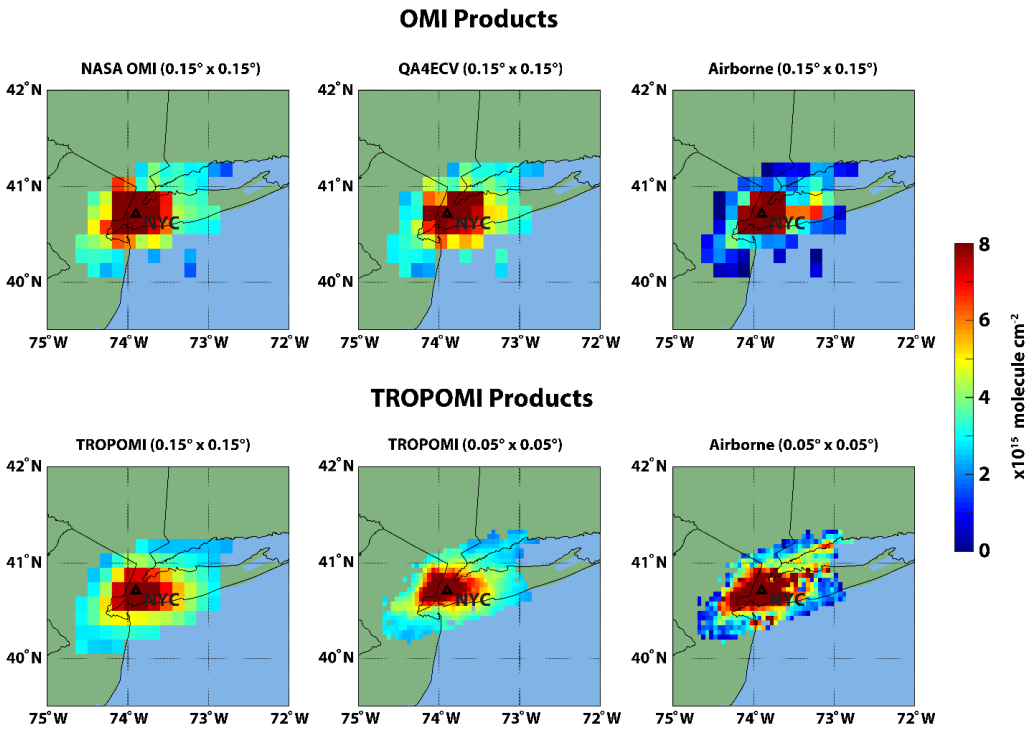

Figure S2: NASA OMI, QA4ECV OMI, TROPOMI, and airborne tropospheric column NO_2 retrievals averaged for all flights conducted during the field campaign. All co-located OMI satellite and airborne remote-sensing tropospheric column NO_2 values are averaged at a 0.15° × 0.15° resolution and co-located TROPOMI data are averaged at both 0.05° × 0.05° and 0.15° × 0.15° spatial resolutions. The black triangle indicates the location of the city of NYC.

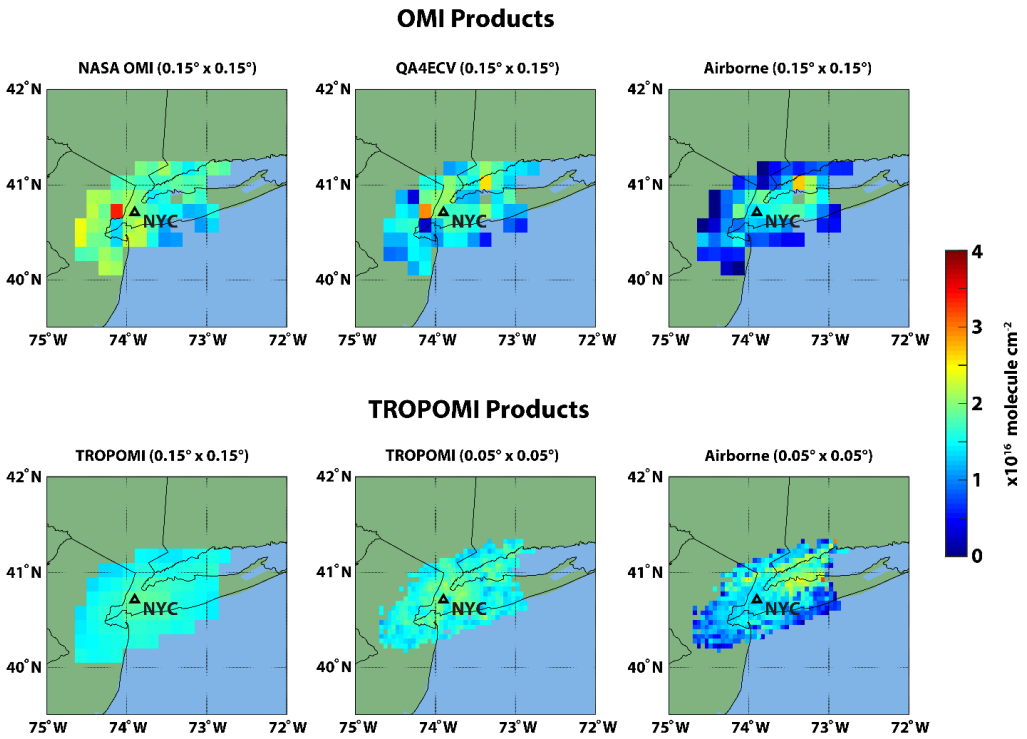

Figure S3: NASA OMI, QA4ECV OMI, TROPOMI, and airborne tropospheric column HCHO retrievals averaged for all flights conducted during the field campaign. All co-located OMI satellite and airborne remote-sensing tropospheric column HCHO values are averaged at a 0.15° × 0.15° resolution and co-located TROPOMI data are averaged at both 0.05° × 0.05° and 0.15° × 0.15° spatial resolutions. The black triangle indicates the location of the city of NYC.

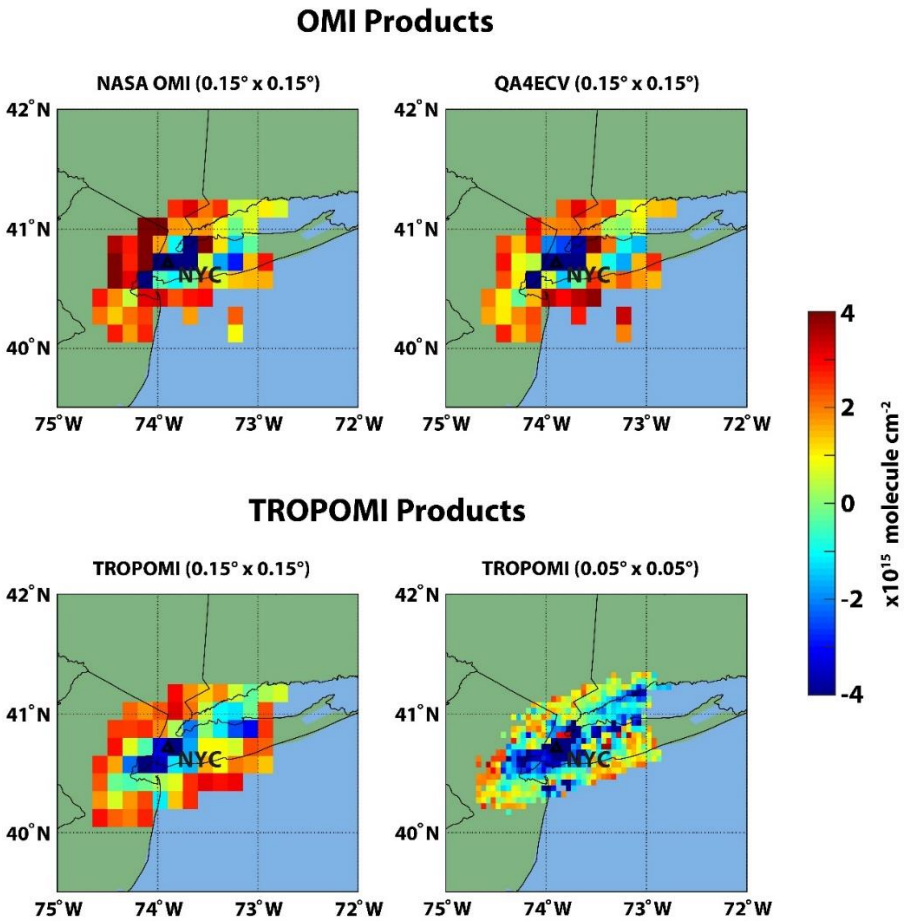

Figure S4: NASA OMI, QA4ECV OMI, and TROPOMI biases in tropospheric column NO_2 retrievals averaged for all flights conducted during the field campaign. All OMI satellite bias values compared to airborne remote-sensing tropospheric column NO_2 values are averaged at a 0.15° × 0.15° resolution and TROPOMI data are averaged at both 0.05° × 0.05° and 0.15° × 0.15° spatial resolutions. The black triangle indicates the location of the city of NYC.

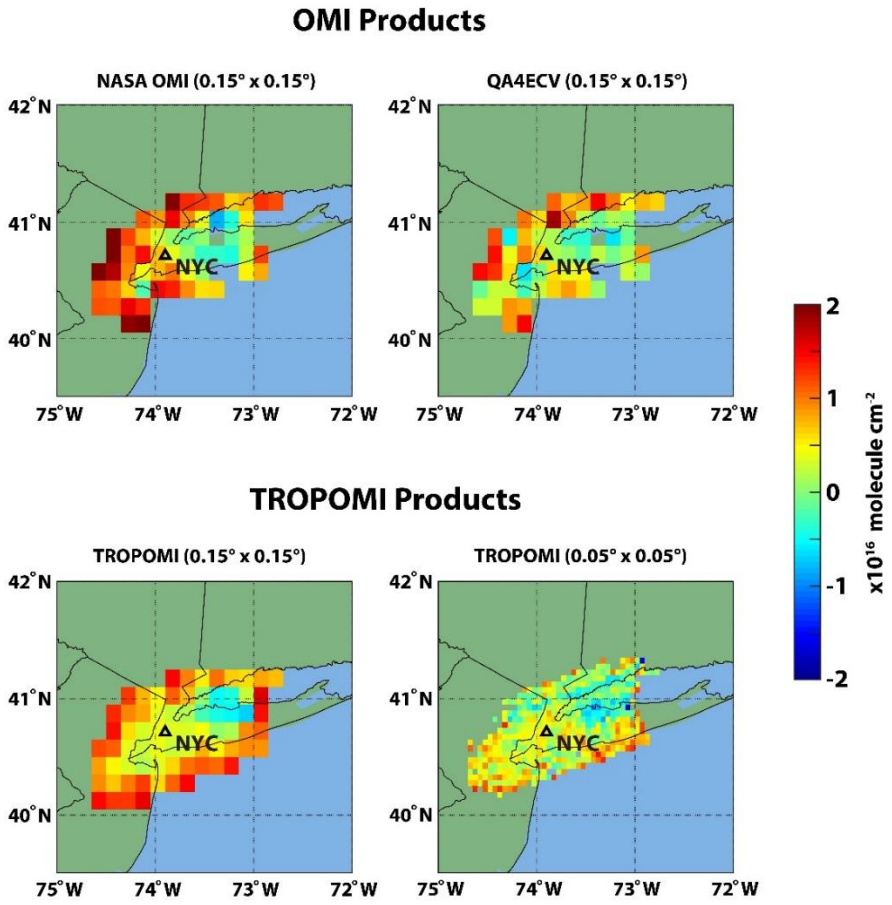

Figure S5: NASA OMI, QA4ECV OMI, and TROPOMI biases in tropospheric column HCHO retrievals averaged for all flights conducted during the field campaign. All OMI satellite bias values compared to airborne remote-sensing tropospheric column HCHO values are averaged at a 0.15° × 0.15° resolution and TROPOMI data are averaged at both 0.05° × 0.05° and 0.15° × 0.15° spatial resolutions. The black triangle indicates the location of the city of NYC.

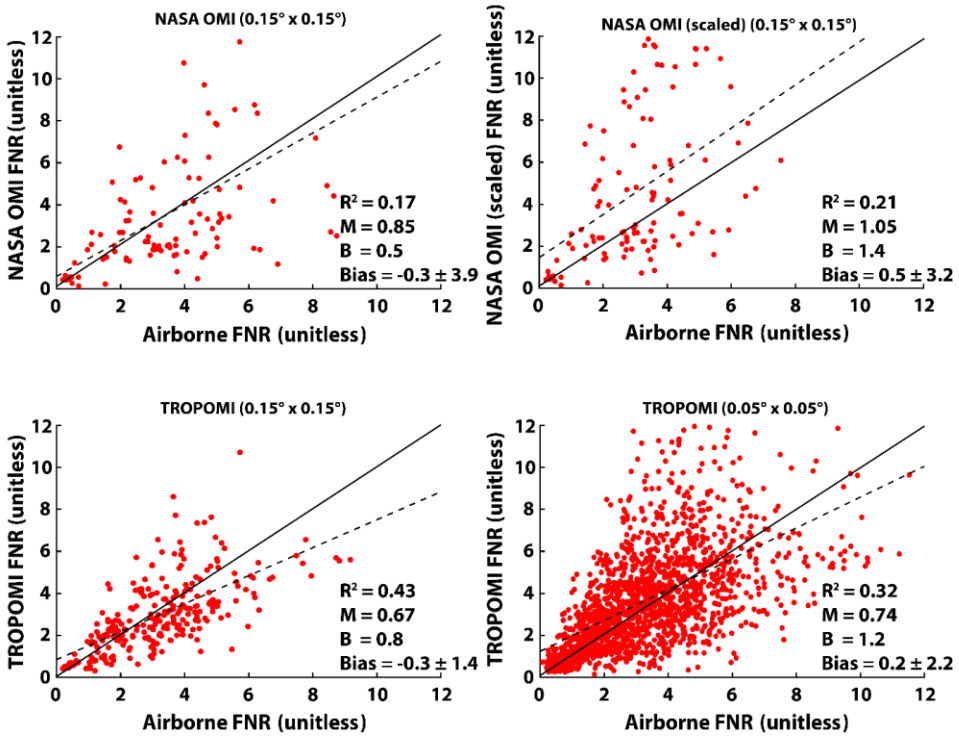

Figure S6: Comparison of satellite (NASA OMI and TROPOMI) reprocessed tropospheric column FNRs and airborne-retrieved tropospheric FNR (unitless) for each co-located measurement taken during the field campaigns. The OMI FNR retrievals calculated with the scaled WRF-CMAQ profiles are identified in the y-axis and titles as "scaled". The solid black line shows the 1:1 comparison and the dashed line shows the linear regression fit. The figure inset shows the main statistics (coefficient of determination (R^2), slope (M), y-intercept (B), and median bias and bias standard deviation) of the comparison.

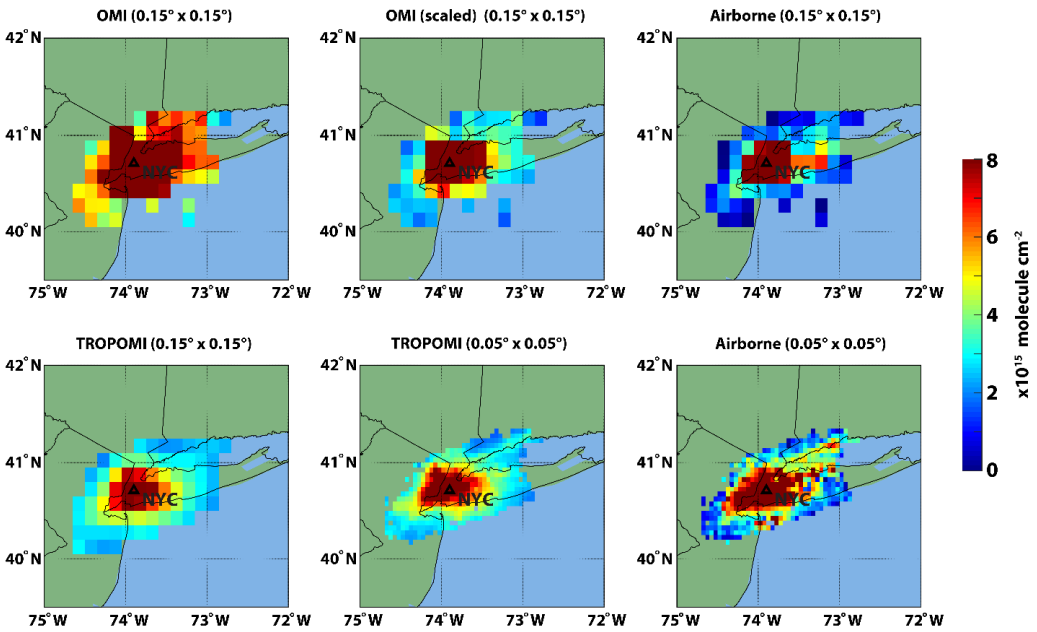

Figure S7: NASA OMI and TROPOMI reprocessed retrievals of tropospheric column NO_2 and airborne observations averaged for all flights conducted during the field campaign. All co-located satellite and airborne remote-sensing tropospheric column NO_2 values are averaged at 0.15° × 0.15° for the OMI intercomparison and 0.05° × 0.05° spatial resolution for TROPOMI. The OMI tropospheric column NO_2 retrievals calculated with the scaled WRF-CMAQ profiles are identified in the titles as "scaled". The black triangle indicates the location of the city of NYC.

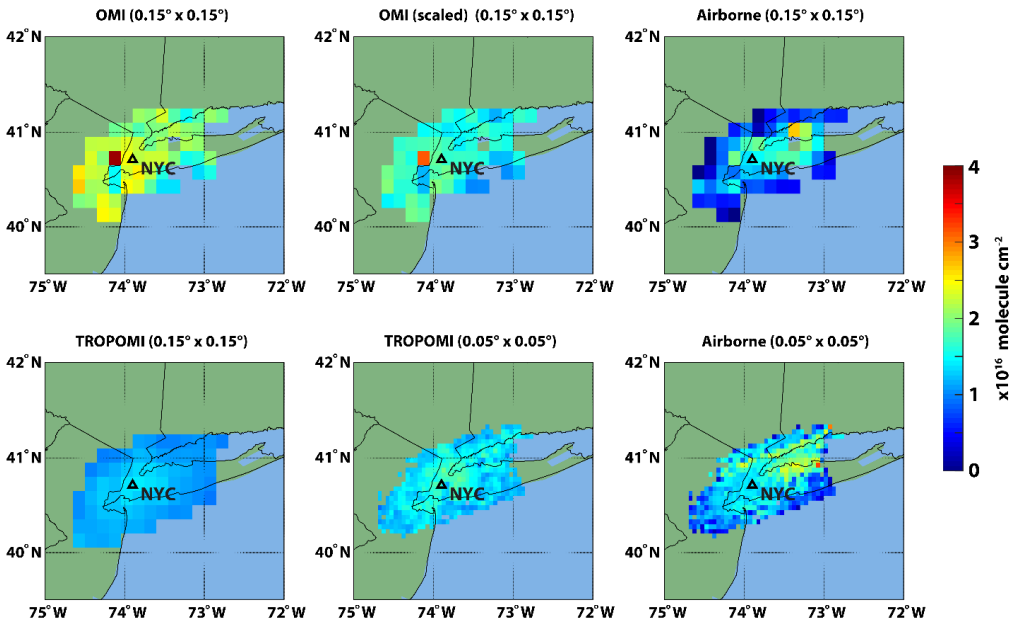

Figure S8: NASA OMI and TROPOMI reprocessed retrievals of tropospheric column HCHO and airborne observations averaged for all flights conducted during the field campaign. All co-located satellite and airborne remote-sensing tropospheric column HCHO values are averaged at 0.15° × 0.15° for the OMI intercomparison and 0.05° × 0.05° spatial resolution for TROPOMI. The OMI tropospheric column HCHO retrievals calculated with the scaled WRF-CMAQ profiles are identified in the titles as "scaled". The black triangle indicates the location of the city of NYC.

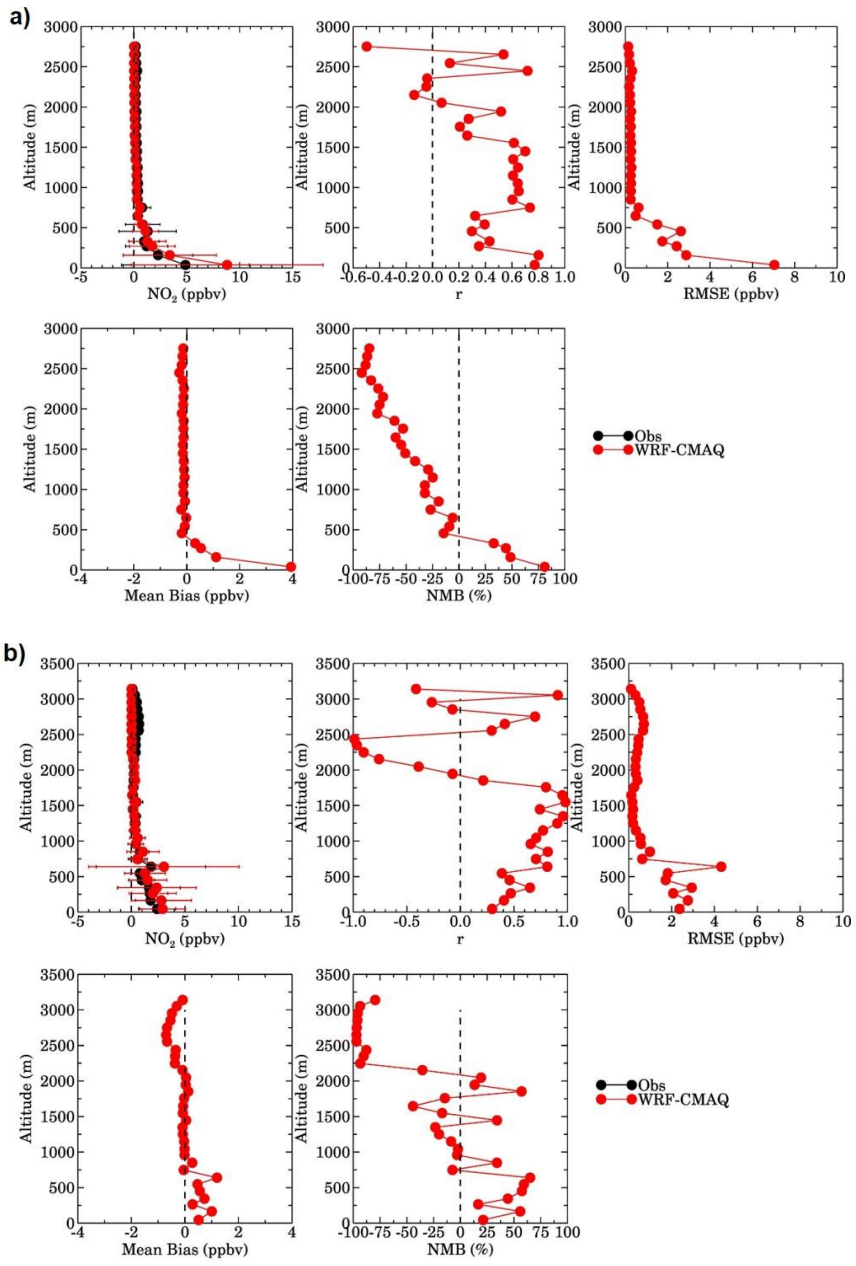
a)
Altitude (m)
NO2 (ppbv)
r
RMSE (ppbv)
Mean Bias (ppbv)
NMB (%)
Obs
WRF-CMAQ
b)
Altitude (m)
NO2 (ppbv)
r
RMSE (ppbv)
Mean Bias (ppbv)
NMB (%)
Obs
WRF-CMAQ

56

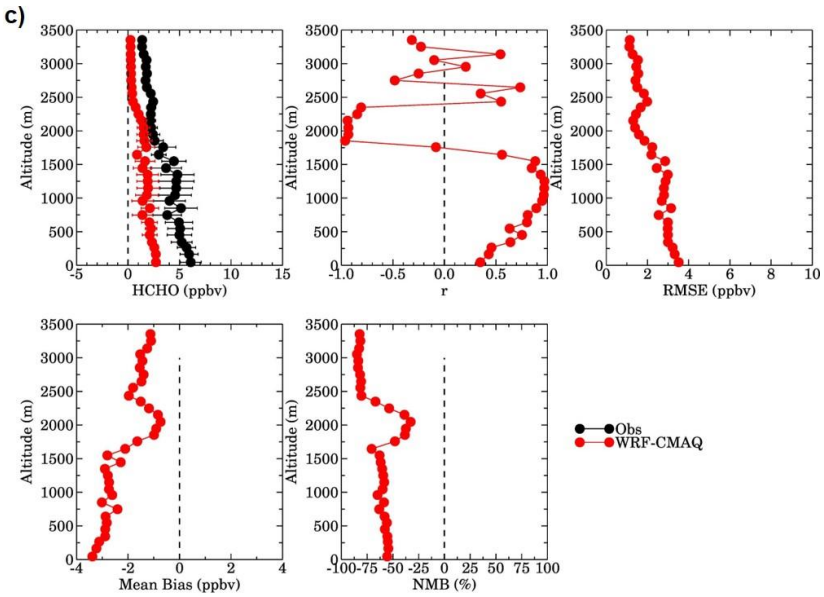

Figure S9: WRF-CMAQ-predicted concentrations (ppb) of NO_2 evaluated with airborne observations during a) OWLETS-2 and b) LISTOS 2018 and c) WRF-CMAQ-predicted HCHO data during LISTOS 2018. The model (red dots/line) and airborne observations (black dots/line) are averaged at 100 m vertical resolution for all measurements during each field campaign. The statistics of the comparison are presented as well.

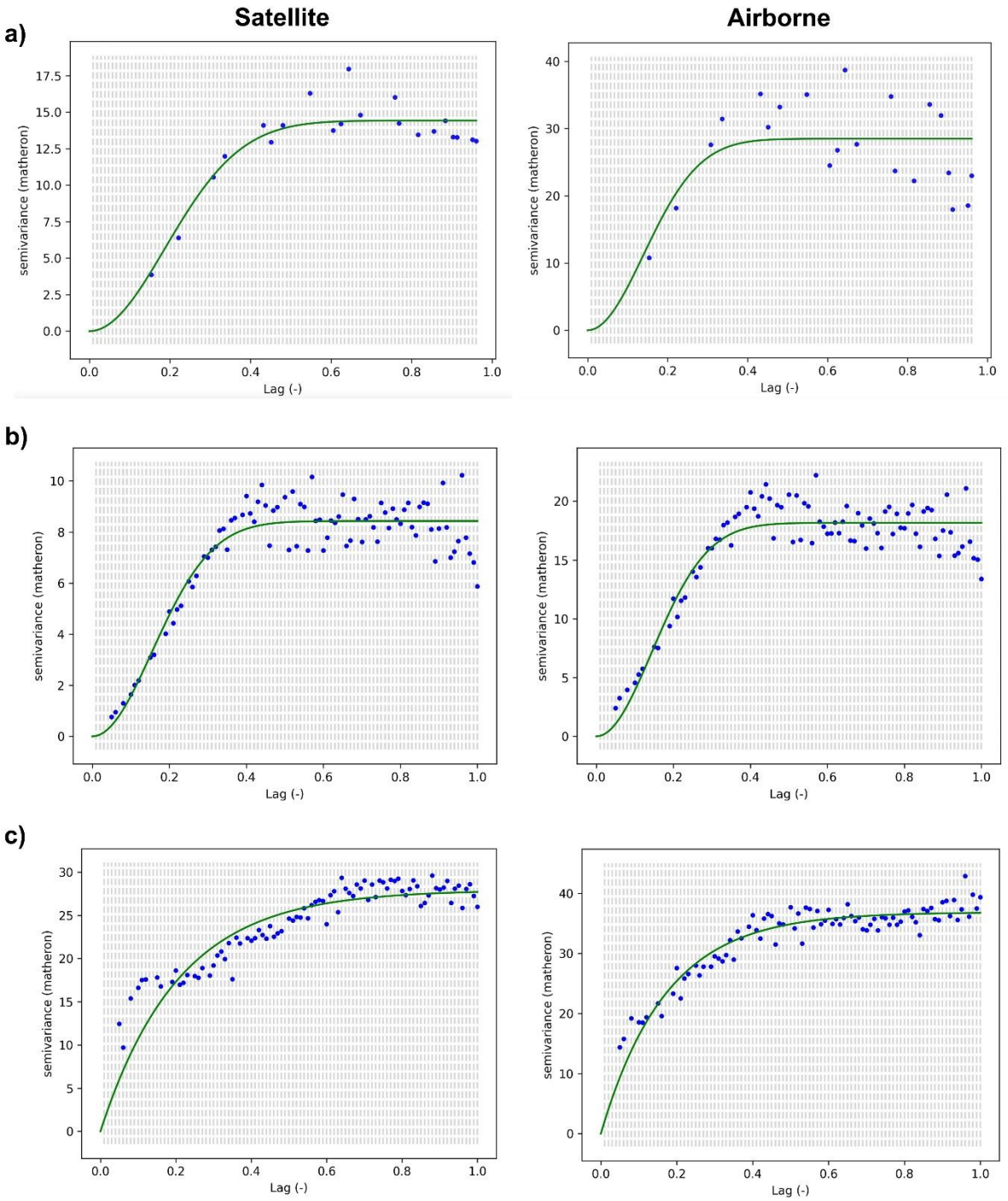

Figure S10: Semivariograms and the fitted stable Gaussian functions for a) TROPOMI NO_2, b) NASA OMI NO_2, and c) TROPOMI HCHO compared to airborne columns. Note the variation between y-axis values in the figure panels.

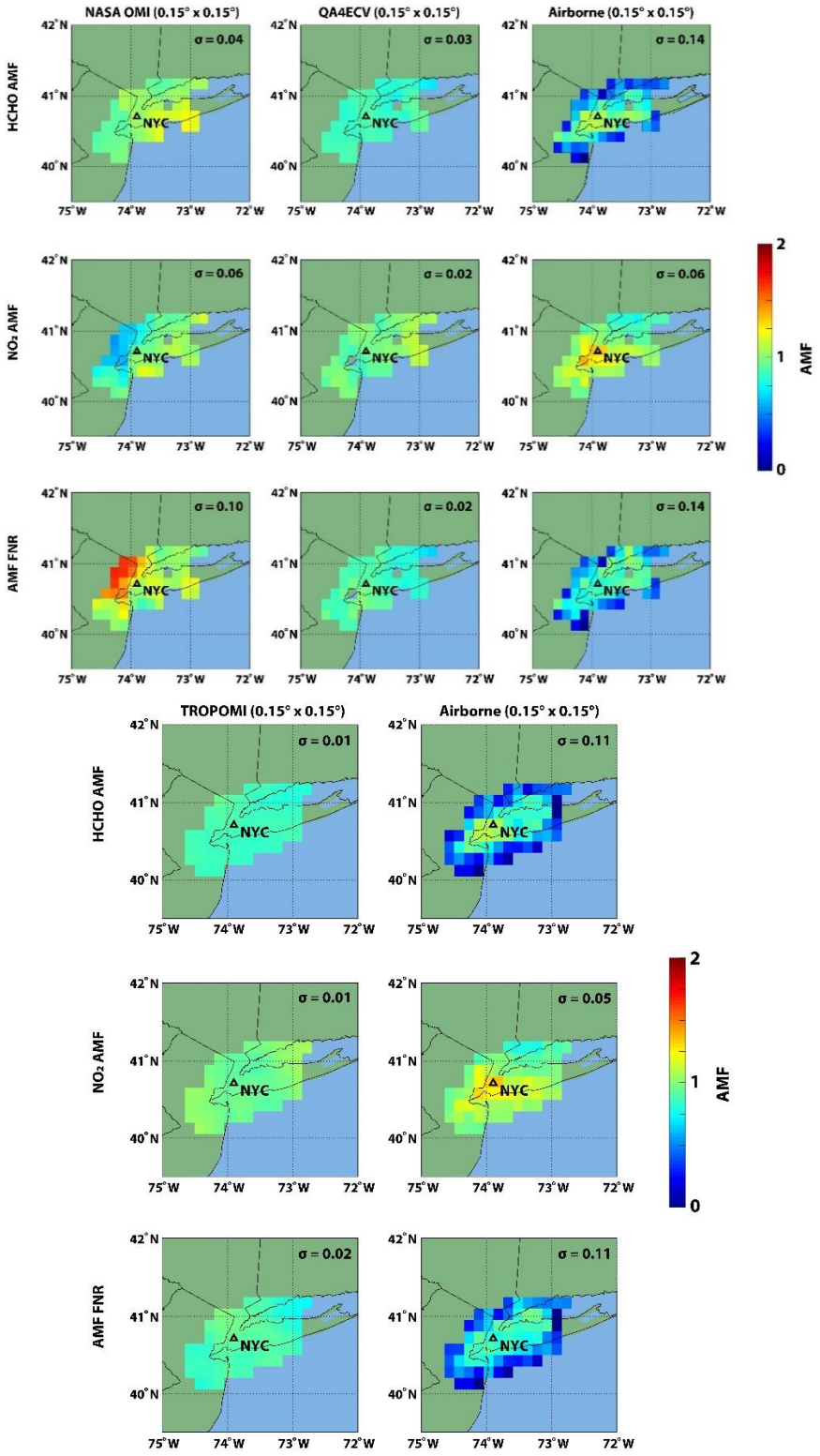

Figure S11: HCHO and NO_2 AMFs, and the resulting ratios of the HCHO and NO_2 AMFs (FNR AMFs), from NASA OMI, QA4ECV OMI, TROPOMI, and airborne retrievals averaged for all flights conducted during the field campaign. All co-located satellite and airborne remote-sensing AMFs are averaged at 0.15° × 0.15° spatial resolution. The black triangle indicates the location of the city of NYC. The figure inset illustrates the standard deviation (σ) of the campaign-averaged AMF values.

References

Iacono, M. J., Delamere, J. S., Mlawer, E. J., Shephard, M. W., Clough, S. A., and Collins, W. D.: Radiative forcing by long-lived greenhouse gases: Calculations with the AER radiative transfer models, J. Geophys. Res., 113, D13103, doi:10.1029/2008JD009944, 2008.

Kain, J. S.: The Kain–Fritsch convective parameterization: An update, J. Appl. Meteor., 43, 170–181, https://doi.org/10.1175/1520-0450(2004)043<0170:TKCPAU>2.0.CO;2, 2004.

Morrison, H., Thompson, G., and Tatarskii, V.: Impact of Cloud Microphysics on the Development of Trailing Stratiform Precipitation in a Simulated Squall Line: Comparison of One- and Two-Moment Schemes, Mon. Weather Rev., 137, 991–1007, https://doi.org/10.1175/2008MWR2556.1, 2009.

Pleim, J. E. and Xiu, A.: Development and Testing of a Surface Flux and Planetary Boundary Layer Model for Application in Mesoscale Models, J. Appl. Meteorol., 34, 16–32, https://doi.org/10.1175/1520-0450-34.1.16, 1995.

Pleim, J. E.: A Simple, Efficient Solution of Flux–Profile Relationships in the Atmospheric Surface Layer, J. Appl. Meteorol. Clim., 45, 341–347, https://doi.org/10.1175/JAM2339.1, 2006.

Pleim, J. E.: A combined local and nonlocal closure model for the atmospheric boundary layer. Part I: Model description and testing, J. Appl. Meteorol. Clim. 46, 1383-1395, https://doi.org/:10.1175/JAM2539.1, 2007.